Characterisation of a phantom for multiwavelength quantitative photoacoustic imaging

2016 Phys. Med. Biol. 61 4950

(http://iopscience.iop.org/0031-9155/61/13/4950)

OPEN ACCESS
IOP Publishing | Institute of Physics and Engineering in Medicine Physics in Medicine & Biology
Phys. Med. Biol. **61** (2016) 4950–4973 doi:10.1088/0031-9155/61/13/4950

Characterisation of a phantom for multiwavelength quantitative photoacoustic imaging

M Fonseca[1], B Zeqiri[2], P C Beard[1] and B T Cox[1]

[1] Department of Medical Physics and Biomedical Engineering, University College London, Gower Street, London WC1E 6BT, UK
[2] National Physical Laboratory, Hampton Road, Teddington, Middlesex TW11 0LW, UK

E-mail: martina.fonseca.13@ucl.ac.uk

Received 12 February 2016, revised 19 April 2016
Accepted for publication 4 May 2016
Published 10 June 2016

Abstract

Quantitative photoacoustic imaging (qPAI) has the potential to provide high- resolution *in vivo* images of chromophore concentration, which may be indicative of tissue function and pathology. Many strategies have been proposed recently for extracting quantitative information, but many have not been experimentally verified. Experimental phantom-based validation studies can be used to test the robustness and accuracy of such algorithms in order to ensure reliable *in vivo* application is possible. The phantoms used in such studies must have well-characterised optical and acoustic properties similar to tissue, and be versatile and stable. Polyvinyl chloride plastisol (PVCP) has been suggested as a phantom for quality control and system evaluation. By characterising its multiwavelength optical properties, broadband acoustic properties and thermoelastic behaviour, this paper examines its potential as a phantom for qPAI studies too. PVCP's acoustic properties were assessed for various formulations, as well as its intrinsic optical absorption, and scattering with added TiO_2, over a range of wavelengths from 400-2000 nm. To change the absorption coefficient, pigment-based chromophores that are stable during the phantom fabrication process, were used. These yielded unique spectra analogous to tissue chromophores and linear with concentration. At the high peak powers typically used in photoacoustic imaging, nonlinear optical absorption was observed. The Grüneisen parameter was measured to be $\Gamma = 1.01 \pm 0.05$, larger than typically found in tissue, though useful for

increased PA signal. Single and multiwavelength 3D PA imaging of various fabricated PVCP phantoms were demonstrated.

Keywords: phantoms, quantitative photoacoustic imaging, polyvinyl chloride plastisol, acoustic properties, optical scattering, optical absorption, Grüneisen parameter

(Some figures may appear in colour only in the online journal)

1. Introduction

Photoacoustic imaging (PAI) is a biomedical imaging modality currently of great interest as it can achieve the fine spatial resolution of ultrasound whilst benefiting from the spectroscopic specificity of optical techniques. It has the potential to recover 3D, high resolution maps providing information on physiology, pathology and function, but one hurdle remains: it is difficult to obtain reliably accurate *quantitative* estimates of the tissue chromophore concentrations. Quantification in PAI is non-trivial because photoacoustic (PA) images, while dependent on the presence of optical absorption for contrast, are proportional to the product of the absorption coefficient and the light fluence, neither of which is known *a priori*. As the fluence is a function of the absorption coefficient, the inverse problem of extracting the concentrations is non-linear and, as the optical scattering is also typically unknown, may be ill-posed (Beard 2011, Cox *et al* 2012). Many approaches have been proposed to address this challenge (Cox *et al* 2009, Pulkkinen *et al* 2014, Shao *et al* 2014, Gao *et al* 2015)—and extensively reviewed in Cox *et al* (2012)—but few have been thoroughly validated and optimised experimentally, much less implemented reliably *in vivo*. A quantitative photoacoustic imaging (qPAI) framework suitable for preclinical/clinical applications needs not only to give accurate and precise estimates, but also be valid for a wide range of scenarios and display robustness to experimental uncertainties and noise. Importantly, validity over the full range of conditions in which the method will be applied should be thoroughly tested and validated experimentally. One impediment to experimental validations is the lack of a well-characterised and detailed phantom material that has both acoustic and optical properties similar to tissue, which is proving to be ever more important as theoretical qPAI strategies improve towards quantification at higher-dimensionality and resolution.

This paper explores what properties the ideal phantom for quantitative PAI would have (section 2) and considers whether PVCP—currently used for non-quantitative PAI validations—could be a suitable material. Section 3 details the PVCP fabrication process. The characterisation of PVCP's acoustic and optical properties are described in sections 4 and 5 respectively, including a study on the effect of high peak power laser pulses typically used in PAI, section 5.3. The measurement of PVCP's Grüneisen parameter is described in section 6. Section 7 shows photoacoustic images obtained using PVCP as a phantom, and a discussion section (section 8) concludes the paper.

2. Phantoms for quantitative photoacoustic imaging

An ideal phantom for photoacoustic imaging (PAI) should possess: (i) tissue-realistic and controllable acoustic properties; (ii) tissue-realistic, stable and controllable optical parameters; (iii) tissue-realistic values for relevant thermoelastic properties; (iv) realistic and

versatile architecture; (v) photo- and mechanical stability during the imaging acquisition procedure; (vi) long-term stability under storage and repeated use; (vii) reproducibility of fabrication.

Up to now, there has been no extensive review of PA phantoms, but some studies have focussed on characterising specific materials for quality control or system assessment in PA, though not directly on their use for quantification (Kharine *et al* 2003, Spirou *et al* 2005, Cook *et al* 2011, Bohndiek *et al* 2013, Vogt *et al* 2016). The studies involve a range of tests such as acoustic characterisation of sound speed, attenuation or backscatter, tuning of optical scattering, tuning of optical absorption and/or the construction of phantom geometries to assess image quality parameters such as signal-to-noise ratio (SNR), contrast, uniformity, spatial resolution, among others.

The characterisation of a phantom for qPAI extends beyond what is needed for semi-quantitative and image quality studies. To assess the suitability of a material for high resolution qPAI these further attributes are required:

(i) Acoustics
  (a) Well-characterised broadband frequency dependency of sound speed and acoustic attenuation. PA-generated signals extend to several tens of MHz (Beard 2011) therefore acoustic properties need to be known at high frequencies to be properly accounted/corrected for. It is not crucial that they match soft tissue exactly as long as they can be correctly accounted for, since incorrect estimation compromises the success of high resolution quantification: erroneous sound speed leads to blurring or artefacts in the acoustic reconstruction, whilst incorrect estimation of acoustic attenuation affects the retrieval of the correct amplitude of the initial pressure distribution. Reference values for soft tissue can be found elsewhere (Duck 1990, Azhari 2010).

(ii) Optics
  (a) Each absorber should ideally have an absorption spectrum that is spectrally unique and similar in magnitude and spectral behaviour to biological tissue chromophores or exogenous contrast agents typically found *in vivo*. Also, the number of different absorbers and their spatial distribution in the phantom material should be representative of relevant *in vivo* scenarios (Laufer *et al* 2007). Reference values for biological tissue and exogenous contrast agents can be found elsewhere (Luke *et al* 2012, Jacques 2013).
  (b) The absorbers should be suitable to be embedded/encapsulated in the phantom matrix material of choice;
  (c) The absorbing species should be suitable for qPAI, regarding: (1) μ_a linearity with species concentration; (2) μ_a addition linearity when in combination with other absorbing species; (3) Low propensity for permanent photobleaching (Laufer *et al* 2010, Avigo *et al* 2015); (4) Low propensity for peak power dependent transient effects such as ground-state bleaching (Laufer *et al* 2010); (5) Known effect of the solvent or matrix on the absorption spectrum (Laufer *et al* 2010, Cook *et al* 2011);

(iii) Photoacoustic efficiency
  (a) Well-characterised Grüneisen parameter Γ (thermoelastic efficiency) of the matrix material and its dependence with the inclusion of additives, e.g. optical absorbers (Laufer *et al* 2010). Γ does not need to match soft tissue exactly (higher Γ can actually bring useful gains in SNR) but should be known, since most suggested theoretical qPAI algorithms already assume Γ is either known *a priori* or constant throughout the domain (Cox *et al* 2012). Knowing Γ is also important as ground-truth in inversion frameworks where Γ is included as an additional unknown to be estimated

(Zemp 2010, Mamonov and Ren 2014). Typical Γ values for some tissues can be found in Yao *et al* (2014).

(b) Minimal fluorescent behaviour (low quantum yield) is desirable, such that the thermalised energy is maximised and confounding parameters in the qPAI problem are minimised.

(iv) Suitability for imaging applications

(a) Feasibility of manufacturing and constructing various phantom structures with interest for imaging purposes, beyond classical image quality assessment geometries.

2.1. Candidate materials for qPAI

The various materials that were considered in this study for qPAI are given in table 1, alongside some of their advantages and disadvantages. The relevant information was obtained either from the studies referred to above that assess the use of the material for PA quality control phantoms, or from reviews on acoustic (Culjat *et al* 2010) and optical phantoms (Pogue and Patterson 2006). It should be noted that nominally identical materials may exhibit slightly different properties, especially if different suppliers or preparation techniques have been used. Materials such as polyester resin and epoxy resin, despite being popular optical phantom options due to their optical transparency and long term stability (Firbank *et al* 1995, Pogue and Patterson 2006), are not appropriate for photoacoustics due to their high sound speed and attenuation, and the support of fast shear waves (Culjat *et al* 2010), and were therefore not included in the list.

2.2. PVCP as a candidate material for qPAI

In this work, PVCP was chosen as the phantom material to be further characterised for qPAI, given its promising long-term stability, optical transparency and tissue-like acoustic properties. Spirou *et al* (2005) first suggested its use for PA, and it has more recently been proposed as a strong candidate for commercial PA system characterisation and quality control (Bohndiek *et al* 2013, Vogt *et al* 2015a, 2016). PVCP has also been considered for other applications, e.g. as a phantom material in optical coherence tomography (Wróbel *et al* 2015) or ultrasound-guided needle insertion (Hungr *et al* 2012).

Some optical properties of PVCP have been previously characterised at single (Spirou *et al* 2005, Bykov *et al* 2011, Bohndiek *et al* 2013) and more recently at multiple wavelengths (Vogt *et al* 2015b). Absorption has been tuned through the addition of black pigment colour, whilst reduced scattering has been increased mainly through the dispersion of titanium dioxide (TiO_2), though zinc oxide (ZnO) has also recently been suggested as an alternative scatterer, in the context of the development of an optical coherence tomography phantom (Wróbel *et al* 2015). Speed of sound and acoustic attenuation have been characterised at low frequencies for commercial PVCP formulations (Spirou *et al* 2005, Hungr *et al* 2012). Acoustic backscatter, the major source of contrast for conventional ultrasound, has been estimated for PVCP with added microspheres (Vogt *et al* 2016). It has also recently been shown that by using custom-made dispersions of PVC in various plasticiser types, a wider range of sound speed and acoustic attenuation values could be obtained (Vogt *et al* 2016). The use of PVCP—or in fact any material—for the assessment and validation of qPAI has nevertheless not been explicitly addressed and investigated.

Table 1. Advantages and disadvantages of several background media materials, in the context of photoacoustic imaging.

Matrix	Advantages	Disadvantages
Water/Coupling-gel	• Easily obtainable; • Largely optically transparent; • Well defined optical and acoustic properties; • Sound speed similar to biological tissue, though somewhat lower (Culjat *et al* 2010)	• Cannot be used to easily sustain an insert; • Does not allow tuning acoustic properties; • Speed of sound varies significantly with temperature (Culjat *et al* 2010); • Allows only reduced flexibility in architecture—shape, layering.
Hydrogels e.g. agar, bovine gelatin (Laufer *et al* 2010, Cook *et al* 2011)	• Solidity for suspending inserts or scattering particles; • Can have dye absorbers added to it; • Largely optically transparent, with the precise levels dependent on the base material used; • Tissue-like speed of sound. • Relative ease of preparation.	• Concentration range typically used significantly affects sound speed (Laufer *et al* 2010); • Well-defined inserts are short-lasting due to diffusion; • Absorption of water; Water soluble dyes need encapsulation (Bohndiek *et al* 2013); • Reaction with nickel and copper ions, changing optical absorption (Laufer *et al* 2010); • Differing dye optical absorption in solution from absorption in gelatin (Cook *et al* 2011); • Cross-linking time; • Susceptibility to dehydration and bacterial growth in storage, thus requiring additional careful mitigating measures (Culjat *et al* 2010, Cook *et al* 2011); • High susceptibility to physical damage (Culjat *et al* 2010); • Low temperature stability at physiological temperatures, causing structural integrity loss; • Limited re-use capability, heavily conditioned by imaging, handling and storage conditions (Culjat *et al* 2010).
Polyvinyl alcohol (PVA) (Kharine *et al* 2003, Xia *et al* 2011)	• Solidity for suspending scatterers or absorbers; • Adjustable intrinsic μ_s; • Tissue-like speed of sound; • Greater longevity and structural rigidity than hydrogels;	• Extensive preparation (several freeze-thaw cycles spanning each several hours) (Culjat *et al* 2010); • Sensitive to humidity (Culjat *et al* 2010); • Inhomogeneities due to differential heating and cooling rates (Xia *et al* 2011).

(*Continued*)

Table 1. (*Continued*)

Matrix	Advantages	Disadvantages
Polyvinyl chloride plastisol (PVCP) (Spirou *et al* 2005, Bohndiek *et al* 2013)	• Solidity for suspending scatterers or absorbers; • Insoluble in water; • Largely optically transparent; • Tunable acoustic properties: hardener/softener; • Stable during storage, up to 6 months (Bohndiek *et al* 2013); • Can be used and re-used for imaging.	• Non trivial preparation; • 180 °C temperature needed for preparation might cause dye denaturation so only pigments should be used; • Higher acoustic attenuation than tissue; • Lack of a widely available supply chain by reference chemical suppliers.
Silicone e.g. room-temperature vulcanising (RTV), polydimethylsiloxane (PDMS) (Avigo *et al* 2015)	• Solidity for suspending scatterers or absorbers; • Insoluble in water; • Can be embedded with inorganic optical scatterers and absorbers; • Capacity to be embedded with acoustic scatterers like e.g. glass an plastic microspheres; • Stable during storage; • Can be used and re-used for imaging; • Variable Young's modulus (hardness), englobing biological tissue levels; • Relative ease of preparation. • For PDMS: Machineability and capability of creating microfluidic channels	• Limited by high acoustic attenuation (>9.8 @ 3 MHz,>39 @ 11 MHz) (Tsou *et al* 2008) and low speed of sound (<1000 ms^{-1}) (Culjat *et al* 2010); • Organic dyes might not be suitable for addition (Pogue and Patterson 2006); • For RTV: Cost (Pogue and Patterson 2006); • Hardening time.

3. PVCP fabrication

The fabrication of PVCP phantoms was based on a previously reported protocol outlined by Bohndiek *et al* (2013). The main steps in the procedure were: (i) prepare an oil bath, heated to ~200 °C, on a magnetic stirrer heating plate; (ii) pour 30 ml PVCP (Lure Flex Firm, Lure Factors, Doncaster, UK) into an Erlenmeyer flask alongside a magnetic stirrer bar; (iii) place the Erlenmeyer in the oil bath and allow it to stir continuously; (iv) turn on the vacuum line connected to the neck of the Erlenmeyer to eliminate air bubbles; (v) as viscosity and

translucency increase, reduce stirring speed; (vi) once the mixture becomes liquid again and considerably transparent, restore initial stirring speed; (vii) when PVCP reaches ~180 °C and the solution is homogeneous (single phase), release the vacuum and swiftly pour PVCP into an alluminium or silicone mould; (viii) Leave it to cure for several minutes.

The addition of optical absorbers or scatterers were used to tune the properties of PVCP. These were mixed together with the PVCP mixture, placed in a sonicator for 10 min to ensure maximum homogenisation, and only then put in the oil bath.

Though the volume of PVCP fabricated and its level of hardness can be increased to suit specific needs, maintaining a homogeneous single phase over time becomes increasingly challenging.

4. Sound speed and acoustic attenuation

PVCP was characterised in terms of its frequency-dependent sound speed $c(f)$ and attenuation $\alpha(f)$. By varying the composition through the addition of a softener agent (Softener, Lure Factors, Doncaster, UK) at either 5, 10 or 20%v/v, the potential to tune the acoustic properties was assessed. Samples of two thicknesses were manufactured (10 and 20 mm, two specimens each). Furthermore, two 2 mm thick samples were prepared for the softest formulation only to extend the range of frequencies. Spirou *et al* (2005) showed that optical additives such as TiO_2 and pigment based absorbers did not significantly affect the acoustic properties, therefore these formulations were not fabricated.

$c(f)$ and $\alpha(f)$ were measured with a through-transmission substitution setup available at the National Physical Laboratory (NPL), UK (Zeqiri *et al* 2010). A broadband transducer (active diameter 12 mm, Medicoteknisk Institute, Denmark) was used as a source and driven by a single cycle electrical pulse with central frequency 9 MHz at a pulse repetition frequency of 1 kHz. Detection was performed with a broadband hydrophone (30 mm active element diameter bilaminar membrane hydrophone, Marconi). Both the hydrophone and the transducer were submerged in a water tank, and aligned.

For each manufactured specimen, measurements were made with and without the sample in the sample holder within the water tank (figure 1). In each case, four oscilloscope readings were taken, where each consisted of an average of 100 waveforms. This procedure was repeated with the hydrophone at 3 distances from the source.

From the measured difference in phase of the detected acoustic wave when the sample is present, $\phi_m(f) = 2\pi f\left(\frac{L-\Delta x}{c_w} + \frac{\Delta x}{c_m}\right)$, or absent, $\phi_w(f) = 2\pi f\frac{L}{c_w}$, the sound speed of the material can be estimated (Zimmermann and Smith 1983, Zeqiri *et al* 2010):

$$c_m = \frac{2\pi f c_w \Delta x}{2\pi f \Delta x - c_w \mathrm{d}\phi} \tag{1}$$

where Δx is the sample thickness, f is the frequency, L the distance between transducer and receiver, $c_w(f)$ the speed of sound in water (Bilaniuk and Wong 1993) and $\mathrm{d}\phi(f) = \phi_w(f) - \phi_m(f)$ the phase difference.

The same data can also be used to retrieve the acoustic attenuation coefficient α_m. When no sample is present, the measured amplitude is $V_w(f) \propto P_i 10^{-\alpha_w L}$, where P_i is the input pressure and $\alpha_w(f)$ the acoustic attenuation in water (Pinkerton 1949). Once the sample is put in place, the amplitude is given by $V_m(f) \propto TP_i 10^{-[\alpha_w(L-\Delta x)+\alpha_m \Delta x]}$, where T accounts for the transmission losses at the two water-material interfaces. The frequency-dependent transmission-loss (TL) is therefore given by:

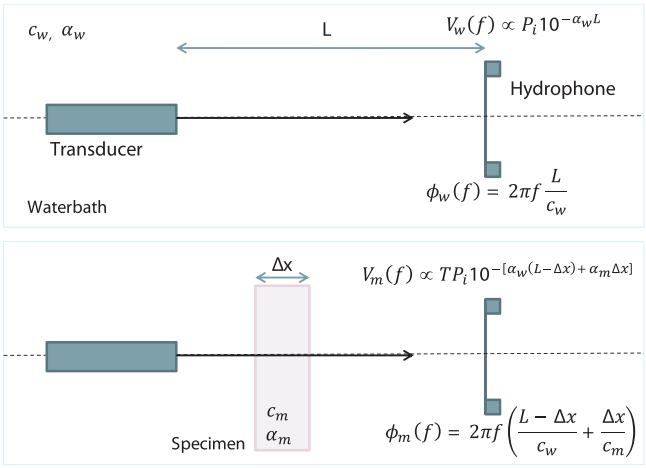

Figure 1. Through-transmission substitution setup used for sound speed and acoustic attenuation measurements.

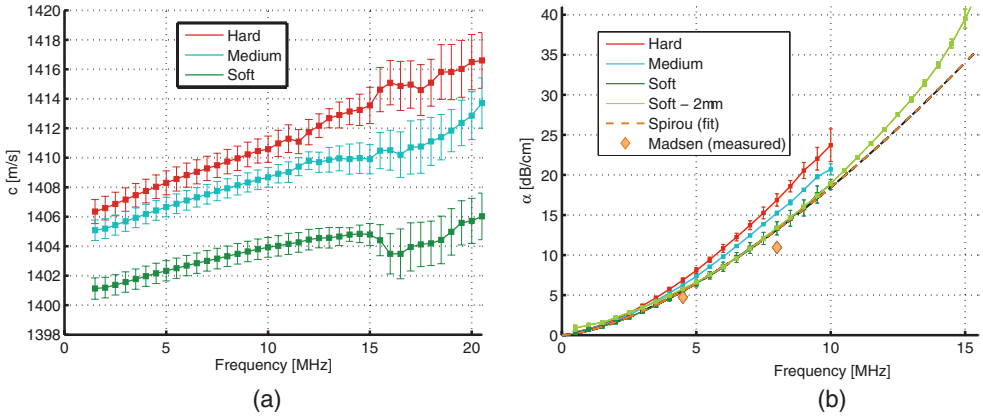

Figure 2. Sound speed (a) and acoustic attenuation (b) for PVCP samples with various levels of hardness. The 2 mm soft PVCP slabs extend the frequency range for $\alpha(f)$ from 10 to 15 MHz.

$$TL\ (\text{dB}) = -20\log\left(\frac{V_w(f)}{V_m(f)}\right) = -20\Delta x(\alpha_m - \alpha_w) + 20\log T. \tag{2}$$

By computing transmission loss for two sample thicknesses Δx_1 and Δx_2, α_m can be retrieved:

$$\alpha\ (\text{dB cm}^{-1}) = \frac{TL(\Delta x_1) - TL(\Delta x_2)}{\Delta x_1 - \Delta x_2} + \alpha_{w\ (\text{dB})}. \tag{3}$$

The frequency-dependent sound speed of PVCP up to 20 MHz and the acoustic attenuation up to 15 MHz are shown in figure 2 and summarised in table 2. The table indicates the

Table 2. Speed of sound and acoustic attenuation, within one standard uncertainty.

Composition	Softener %v/v	Sound speed c (m s^{-1})	Power law pre-factor a (dB cm^{-1} MHz^{-b})	Power law exponent b	Samples #	Temperature (°C)
Hard	5	1408.3 ± 0.8 @ 5 MHz	0.67 ± 0.02	1.55 ± 0.01	4	$(20.5–20.8) \pm 0.03$
Medium	10	1406.7 ± 0.7 @ 5 MHz	0.62 ± 0.03	1.54 ± 0.02	4	$(20.5–20.8) \pm 0.03$
Soft	20	1402.3 ± 0.7 @ 5 MHz	0.55 ± 0.05	1.53 ± 0.01	4	$(20.6–20.9) \pm 0.03$
Spirou *et al* (2005)[a]		1400 ± 20 @ 1 MHz	0.57 ± 1.01	1.51 ± 0.06	3	—
Madsen *et al* (2003)[b]		1395	1.05 dB cm^{-1} MHz^{-1} @ 4.5 MHz		1	22
Vogt *et al* (2015b)[c]		1380–1575	1–30 dB cm^{-1} MHz^{-1} @ 4.0 MHz		—	—

Note. Literature values are given for other PVCP formulations:
[a] MF Manufacturing;
[b] unknown origin;
[c] range of custom formulations.

speed of sound c at 5 MHz and the attenuation behaviour in terms of power law parameters a and b ($\alpha(f) = a f^b$, where f is in MHz). Literature-reported values for PVCP formulations from other suppliers are listed as well for comparison. The reported uncertainty refers to one standard uncertainty, providing a coverage probability of approximately 68% (coverage factor $k = 1$). The uncertainty evaluation has been carried out in accordance with UKAS requirements (UKAS 2012). Uncertainties in sample thickness, temperature, literature reference values for water, repeated measurement variability and inter- and intra-sample variability were accounted for. The speed of sound and attenuation were broadly comparable to tissue-like structures. Nevertheless, c was up to ~10% lower than the typical soft tissue range (e.g. 1450 ms^{-1} for fat or 1590 ms^{-1} for liver (Azhari 2010)). The attenuation at 1 MHz was well within desired tissue range—between 0.6-1 among soft tissues—, nevertheless the power law b was above the typical range of $b = 1$–1.35 (Azhari 2010), which might limit the depth to which high-resolution can be achieved. Increasing hardness through the increase of the relative volume of PVC particles in the plasticiser caused an increase in the sound speed and attenuation, although it remained below the speeds typical of tissue. Further increases in hardness through an even higher relative percentage of PVC particles would cause difficulties in the fabrication process. Recently however, it has been shown that the sound speed can be increased to more tissue-matched levels by using other types of plasticisers to suspend the PVC particles (Vogt *et al* 2015b, 2016), though at the cost of an increasing attenuation that, though suitable for breast tissue up to 9 MHz, would be too high to be representative of most other soft tissues and further limit depth resolution and SNR.

5. Optical properties

PVCP has intrinsic, relatively low, optical scattering and absorption which can be increased using additives.

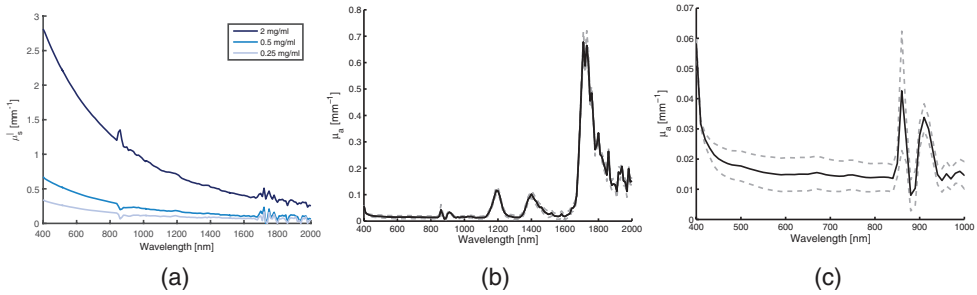

Figure 3. (a) Reduced scattering coefficient spectra of PVCP with varying concentrations of TiO_2. (b)–(c) Intrinsic absorption spectrum of soft PVCP. Variations at 850 nm are in fact artefacts due to the change of detectors within the spectrophotometer. The dashed lines correspond to the standard deviation between the estimated μ_a for the four slabs.

5.1. Optical scattering

Optical scatterers can be used to tune the scattering behaviour towards more tissue-like levels. TiO_2 powder (Titanium IV Oxide, Anatase, 232033, Sigma-Aldrich, Germany) is most commonly used and readily available (Spirou *et al* 2005) and was thus used to fabricate soft PVCP samples (2 mm thick) at 4 different concentration levels—0.25, 0.5 ,1 and 2 mg ml^{-1}. Integrating sphere measurements coupled with the inverse adding-doubling (IAD) algorithm (Prahl *et al* 1993) were employed to determine the reduced scattering coefficient μ_s', and simultaneously the intrinsic absorption coefficient μ_a. Total transmittance (M_T) and total reflectance (M_R) measurements were carried out at four different spots on each sample (2 per side) between 400–2000 nm with a 100 mm integrating sphere mounted in a dual-beam spectrophotometer (Lambda 750, Perkin Elmer, Waltham, MA, USA). IAD is an inverse light modelling strategy that recovers μ_s' and μ_a by iteratively finding the adding-doubling solution to the radiative transfer equation (RTE) under the assumption that the sample under study is a layer-like structure where each layer has homogeneous absorption and scattering. The scattering anisotropy factor, necessary as an input parameter, was set to $g = 0.6$, based on Mie Theory calculations from the literature for TiO_2 in PVCP (Bykov *et al* 2010).

The reduced scattering spectra of PVCP with added TiO_2 are given in figure 3(a). Scattering for all samples was found to be comparable to biological tissue in terms of the order of magnitude expected (Jacques 2013). There is an approximate linearity of μ_s' with increasing TiO_2 concentration. It should be noted that the 1 mg ml^{-1} sample that was prepared had visible homogeneity issues likely caused by lack of proper dispersion of the mixture—which was subsequently rectified with increased mixing and sonicating—and its curve has therefore been omitted since it gave an erroneous portrayal of the expected behaviour (curve can be seen in Fonseca *et al* (2015)). The values obtained are in the same range as those in other μ_s' characterisation studies (Bykov *et al* 2010, Vogt *et al* 2015b), but the absolute values differ among them. This is due to the fact that different TiO_2 products can have different particle size distributions and even refractive indices (Phillips and Griffen 1981), and both parameters affect μ_s'. When designing a phantom, care must therefore be taken when referring to scattering measurements using different TiO_2 commercial products. Scattering characterisation should therefore ideally be performed per batch, even for products where the supplier specifies a mean particle size to a high degree of

accuracy. Literature values should rather serve as a guideline for spectral behaviour and for preparing samples in the desired order of magnitude.

5.2. Optical absorption

The intrinsic absorption spectrum of PVCP is shown in figures 3(b) and (c). PVCP has intrinsic absorption peaks at 910, 1190, 1400 and 1720 nm, probably due to vibrational energy transitions (overtones) in PVC (Goddu and Delker 1960). Overall, the absorption is low and analogous in range and magnitude to background biological tissue (Jacques 2013). A standardised preparation of the material is advised (Spirou *et al* 2005, Van de Ven and Erdman 2006) since the absorption may vary to a certain extent with the sample preparation process, namely due to factors such as heating rate and final heating temperature. For example, PVC suffers a significant decrease in optical transmission when held at temperatures in the 190–205°C range (Van de Ven and Erdman 2006).

The absorption of PVCP can be tuned through the use of additives. Pigment dispersions—where pigments are pre-dispersed in a paste and then mixed with softener—are advised as colorants (Berins 1991, Pigments and Additives Division: Clariant International Ltd 2007). Soluble dyes on the other hand are not suitable for use in plasticised PVC formulations since they migrate in the presence of the plasticiser (Pigments and Additives Division: Clariant International Ltd 2007). Three pigment-based absorbers (black, red and blue) from the same supplier as the PVCP (Liquid Colour, Lure Factors, Doncaster, UK) were therefore characterised. 2 mm thick slabs of soft PVCP were fabricated, with added absorbers at 0.5, 0.25 and 0.125%v/v concentration (serial dilution). Their absorption was characterised with the spectrophotometer, with four points being assessed per sample.

Embedding either blue, black or red pigment absorbers in PVCP led to three unique spectra (figures 4(a)–(c)). For all pigments, μ_a was found to be linear with pigment concentration (figures 4(d)–(f)).

5.3. Absorption at high peak power

PA imaging is usually performed using pulsed rather than continuously-modulated illumination. Efficient PA signal generation requires a condition of stress confinement to be satisfied, which requires the use of pulses of $\leqslant$10 ns duration. Since the phantom is meant for photoacoustic imaging, it needs to be able to cope with exposure to high peak power sources. In addition, for imaging systems that require repeated and prolonged pulsed exposure (e.g. reliant on raster scanning for PA acquisition), the ability to withstand the accumulation of average power is necessary.

To investigate the effect of using a high peak power source (as used in PA) rather than a low power continuous wave source (as used in the spectrophotometer), absorption coefficient measurements were made using photoacoustic spectroscopy (Stahl *et al* 2014) (figure 5), on 1%v/v 20 mm slabs of the same fabrication batch as the spectrophotometer samples. A fibre-coupled Nd:YAG pumped wavelength-tunable optical parametric oscillator (OPO) system (GWU, Spectra-Physics, Santa Clara, CA, USA) was used for excitation light delivery, tunable between 500–680 nm and 740–2100 nm and providing 7 ns long pulses at 10 Hz pulse repetition rate. A 10 mm $\times$ 10 mm $\times$ 50 μm polyvinylidene fluoride (PVDF) film bonded to a PMMA backing (Stahl *et al* 2014) was used for acoustic detection of the PA signal. The recorded PA signal $S(t) = \beta\Gamma\Phi_0\mu_a e^{-\mu_a ct}$ [V] can then be used to retrieve μ_a through curve-fitting to the exponential decay, where β is a scaling parameter related to system sensitivity and Φ_0 is the incident fluence. Additionally, a different high peak power

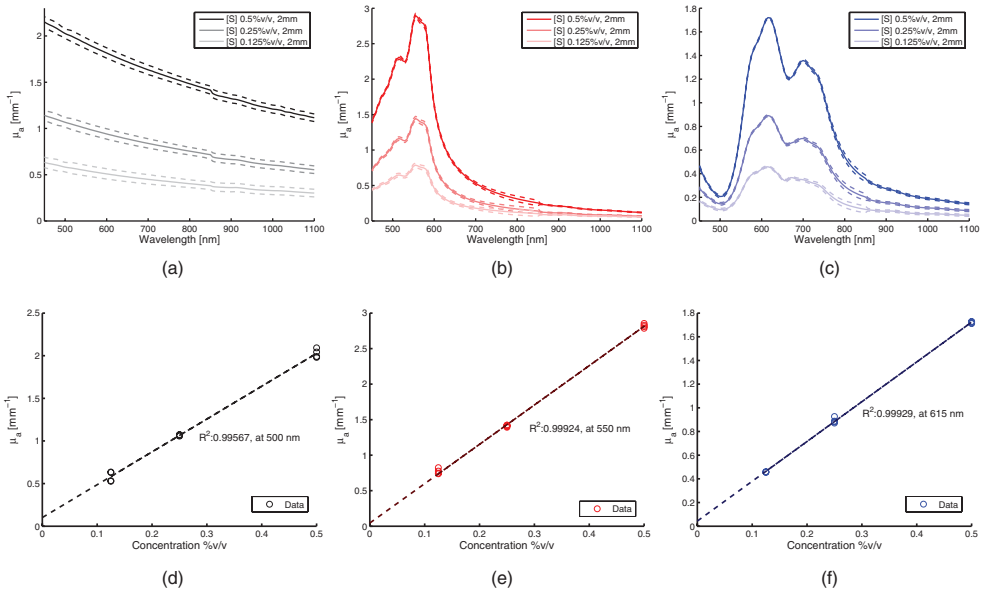

Figure 4. (a)–(c) Absorption spectra of PVCP slabs with embedded absorbers, at different concentrations; [S]—spectrophotometer acquired data. Dashed lines represent the standard deviation of the four measurements on the same sample. (d)–(f) Linearity of spectroscopic μ_a with increasing concentration at the peak wavelength. (a) Black. (b) Red. (c) Blue. (d) Black. (e) Red. (f) Blue.

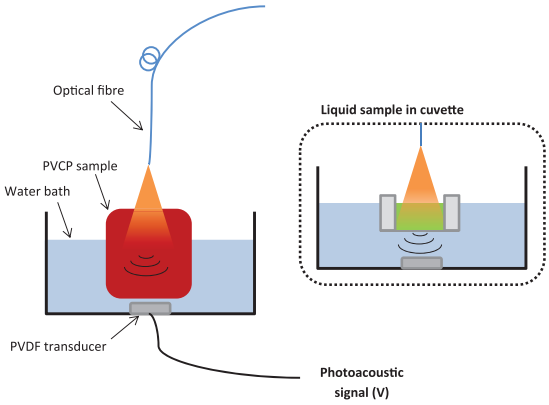

Figure 5. Photoacoustic spectroscopy diagram. The inset shows the case where a liquid sample is imaged in a cuvette, instead of having a PVCP sample placed directly in the water bath.

ns-pulsed laser source (SpitLight 600, Innolas, Krailling, Germany) was also employed to make optical transmission measurements, with the light detection being done by a powermeter (PowerMAX PM10V1, Coherent, Santa Clara, CA, USA). Three repeat measurements were made with the 2 mm slabs used for spectroscopy.

Figures 6(a)–(c) show, for the three absorbers, that spectrometer-derived ([S]) and photoacoustic-derived ([P]) μ_a spectra differ. The red absorber shows the most notorious alteration, since the change in absolute absorption is accompanied by a clear alteration in the shape of

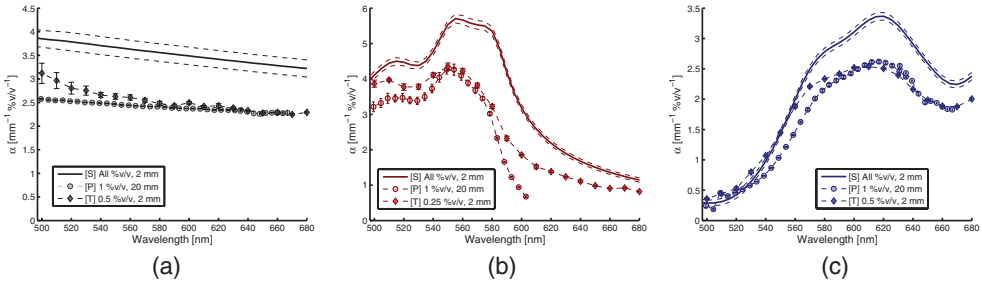

Figure 6. Comparison of extinction coefficient measured through: transmittance in spectrometer [S] (linear regression of results from samples at all concentrations) with cw-illumination, exponential fit of photoacoustic signal [P] and transmittance [T] with a high peak power OPO source. Measurement standard deviation is given. (a) Black. (b) Red. (c) Blue.

the spectrum. The 550–580 nm plateau from the spectroscopic measurements does not appear in the photoacoustically-derived spectrum, giving way to a rather peak-like feature at 550 nm. In addition, the results of transmittance measurements performed with a high peak power source on the 2 mm slabs showed characteristics similar to the photoacoustic measurements (figures 6(a)–(c), [T]). These results seem to indicate that the absorbers may be suffering photochemical or photo-physical changes in behaviour when exposed to high peak power nanosecond pulses (Khairutdinov and Serpone 1995, Marcano *et al* 2000, Berera *et al* 2009, Laufer *et al* 2010, Kislyakov and Yelleswarapu 2013) (∼1 MW peak power) that do not occur when exposed to the low power continuous-wave illumination of the spectrophotometer (∼W peak power).

Control measurements were first made with a $CuCl_2$ solution (previously shown to have transient and permanent photostability (Laufer *et al* 2010)) on both the spectrophotometer and photoacoustic systems, to ensure both systems agreed and were working up to specification in the relevant absorption range. Intrinsic absorption of PVCP (no added pigments) around the 1720 nm peak was also in good agreement between systems. Measurements of water absorption between 1350 and 2000 nm (representing a range of μ_a up to 12 mm^{-1}) were also made with the PA spectroscopy system to ensure that the exponential fitting methodology was accurate compared to literature reference values (Palmer and Williams 1974).

To further study the behaviour of the pigment-embedded PVCP when exposed to high peak power, photoacoustic absorption measurements were made as a function of illumination time, as a function of incident peak energy and as a function of pigment concentration.

The influence of the fluence on μ_a was assessed by obtaining photoacoustic absorption spectra at varying levels of incident fluence—100, 80, 60, 40 and 20% of Φ_{max}, where the non-attenuated energy is ∼27 mJ at 500 nm and ∼16 mJ at 680 nm. In a first experiment, one point on the sample was illuminated with increasing peak energy levels. In a second scenario, a different point was illuminated with decreasing peak energy levels. Finally, an experiment was performed where different points were illuminated with distinct peak energy levels—with minimised common history between points. These three modalities were employed to differentiate effects due to high peak power (leading to transient bleaching) from effects due to the accumulation of average power over an extended time (leading to permanent bleaching).

An increase in energy per pulse led to a decrease in μ_a (figure 7). The decreasing trend in μ_a when fluence is increased gradually over time (figures 7(a) and (d)) could be assigned to permanent photobleaching by accumulation of average power, nevertheless that would not

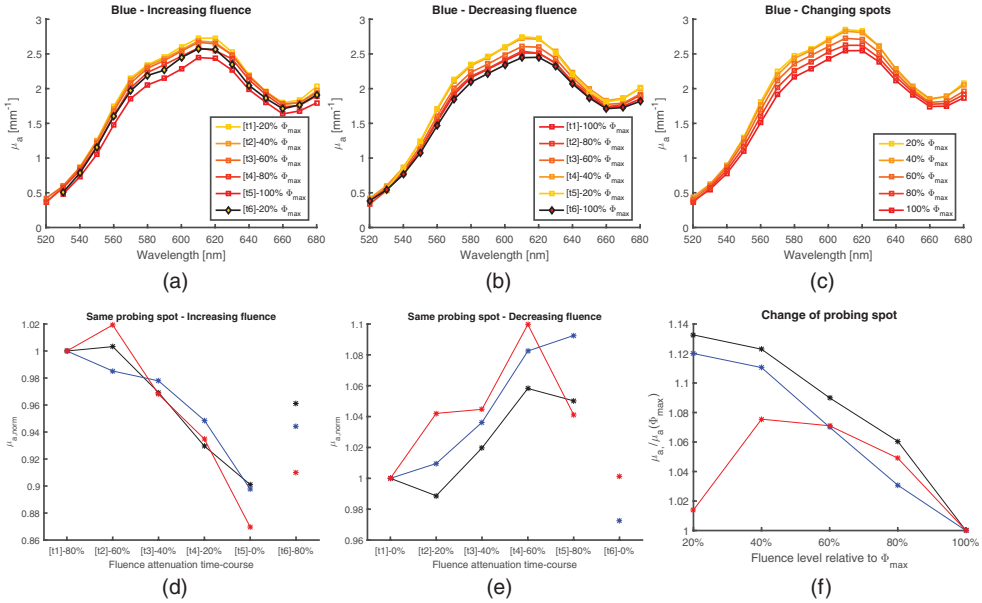

Figure 7. (a)–(c) Influence of varying peak power energy on the μ_a of blue PVCP samples. Results are shown as peak energy is gradually increased over a same location for timepoints [t1–5] and restored to its initial (lowest) value in [t6] (a), as peak energy is gradually decreased over a second location for timepoints [t1–5] and restored to its initial (highest) value in [t6] (b), and as peak energy is varied over distinct locations/spots on a same sample (c). (d)–(f) Influence of varying peak power energy on μ_a of PVCP samples embedded with either of the three colours. Red and black values are shown for 550 nm whilst blue values are shown for 610 nm.

explain why μ_a is partially restored at timepoint [t6] when energy is reset to its lowest level. It also would not explain why when one point is illuminated with gradually decreasing pulse energy the μ_a levels increase (figures 7(b) and (e)). Illuminating different points on a sample with distinct pulse energies also shows that μ_a increases as pulse energy is lowered (figures 7(c) and (f)). This suggests that there is a dependency of μ_a on peak pulse energy, likely due to the transient/reversible occurrence of ground-state bleaching (saturable absorption) (Berera *et al* 2009).

To assess μ_a as a function of extended illumination time, black, red and blue PVCP slabs were continuously irradiated with the Spectra-Physics OPO laser for 30 min, 10 Hz pulse repetition rate, at their respective peak absorption wavelength—500 nm, 550 nm and 615 nm. The average beam energy was 5 mJ. PA signals were averaged over a minute and stored.

The PVCP with embedded pigments displayed reasonable stability over a 30 min irradiation period (18 000 pulses)—data not shown. A decreasing μ_a trend was seen, but it did not exceed 5%. Given the timescale of the measurement and the accumulation of average power, the decrease is probably due to permanent photobleaching. Transient effects such as ground state bleaching or saturable absorption take place in the sub-nanosecond to nanosecond time regime (Khairutdinov and Serpone 1995) as a result of high peak power, thus their temporal onset and trend would not be noticed in this experimental setup.

To assess the linearity of PA-derived μ_a with increasing concentration, a new batch of samples was prepared. Red and blue 20 mm thick PVCP slabs were fabricated at 2, 1 and 0.5%v/v

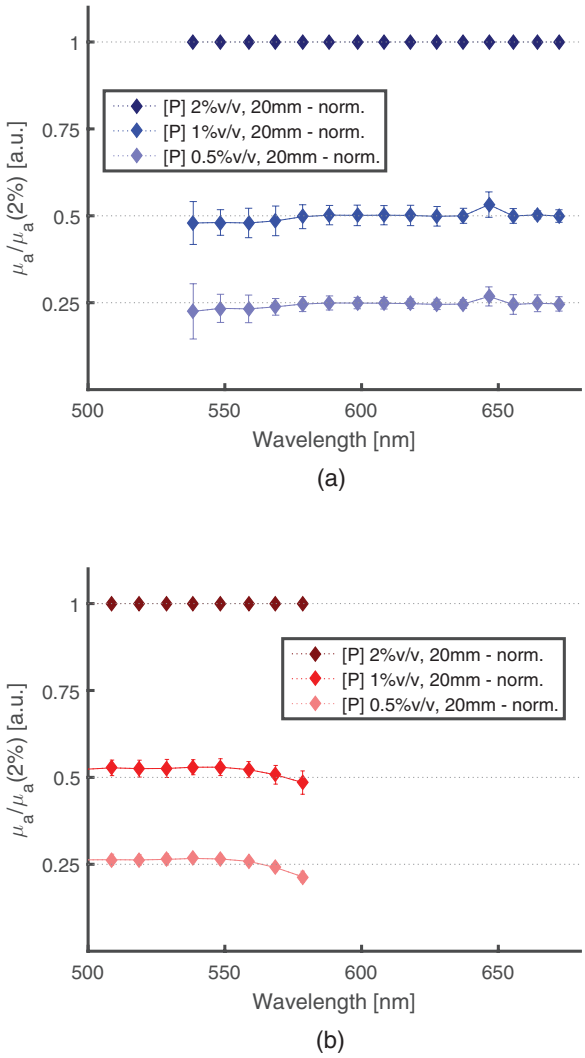

Figure 8. Spectra at different absorber concentrations (0.5, 1 and 2%v/v) normalised to the spectrum at 2 %v/v. 1/2 and 1/4 concentration ratios are broadly respected. Error bars account for inter-acquisition standard deviation and for the standard uncertainty in the exponential fitting procedure. (a) Blue absorber, (b) red absorber.

pigment concentration. 3 acquisitions were made per sample in the 500–680 nm range, each consisting of the averaging of 100 waveforms.

Figure 8 shows the level of linearity of the photoacoustically-derived μ_a with absorber concentration. Spectra have been normalised to the mean spectrum for 2%v/v absorber concentration, and if linearity holds should respect the 1/2 and 1/4 dilution factors. Only wavelengths where the coefficient of correlation of the exponential fit satisfies $R^2 > 0.98$ are shown.

The blue samples display linearity with concentration whilst the red seem to display small deviations from absorption linearity in the 540–580 nm region: the lower the concentration, the lower the relative absorption at 570–580 nm compared to 540–550 nm. This coincides with the observations made when comparing spectrophotometer ([S]) to photoacoustic data ([P])

(figure 6(b)). Saturable absorption manifests itself not only at increasing peak power levels, but also when concentrations are lowered, since this lowers the ratio of absorbing molecules per unit volume to the number of photons.

6. Grüneisen parameter

The Grüneisen parameter Γ quantifies the relationship between the optically absorbed and thermalised optical energy to pressure and has a direct impact on the PA amplitude. Its characterisation is therefore important in a qPAI context and was pursued in this study. The PA spectroscopy system described in the previous section was used, with a method comparative to water being employed to retrieve γ Stahl *et al* (2014). Briefly, PA measurements were made for water and the sample of interest, with fluence-normalised amplitudes defined by $S'_{0,\text{water}} = S_{0,\text{water}}/\Phi_0 = \beta\Gamma_{\text{water}}\mu_{a,\text{water}}$ and $S'_{0,\text{sample}} = S_{0,\text{sample}}/\Phi_0 = \beta\Gamma_{\text{sample}}\mu_{a,\text{sample}}$ respectively. The sensitivity parameter β was retrieved from the PA measurement of water, $S_{0,\text{water}}$, through least-squares regression in the 1350–1850 nm region, where $\mu_{a,\text{water}}$ and Γ_{water} are known from the literature (Haynes 2012, Palmer and Williams 1974). The derived β value, alongside $\mu_{a,\text{sample}}$ values retrieved through curve-fitting at the relevant wavelengths, were then used in the equation for $S_{0,\text{sample}}$ to retrieve Γ_{sample}.

Unlike the case where a water-filled cuvette is placed in the water bath, when other samples are placed there is a considerable acoustic impedance mismatch at the interface with the water bath. This will result in a change in acoustic transmission, given by $T_{\text{s,w}} = \frac{2\,Z_{\text{w}}}{Z_{\text{w}} + Z_{\text{s}}}$, where Z_{w} and Z_{s} are the characteristic acoustic impedances of water and the sample respectively. To correct for this error, the measured amplitude S was divided by the appropriate transmission $T_{\text{s,w}}$ (Yao *et al* 2014). Method validation was carried out with methanol and ethanol, where the reference values were taken from the literature and are shown in table 3.

Methanol, ethanol and water, were poured in turn into a cuvette which was then placed within a water bath. 3 acquisitions were carried out per substance, each acquisition being comprised by the averaging of 300 waveforms. 6 acquisitions were made on a 20 mm slab of PVCP for the 1700–1750 nm region.

Table 3 gives the results of the Grüneisen parameter characterisation. The estimated Γ values for ethanol and methanol are consistent with the literature. Γ of PVCP is higher in value than some tissues (Yao *et al* 2014), though this has as advantage that imaging can be done with higher SNR. Error ranges for the obtained Γ estimates take into account inter-acquisition standard-deviation as well as the standard uncertainty of the least-squares regression process applied to each acquisition.

The variation in Grüneisen parameter with added blue or red pigments was also studied for 20 mm thick PVCP slabs with concentrations of 2, 1 and 0.5%v/v. These measurements were made at a single wavelength where intrinsic PVCP absorption is highest and pigment absorption is residual—1715 nm, which means that measured variations in $S_{0,\text{sample}}$ with pigment concentration will be mainly due to changes in Γ rather than μ_a (Laufer *et al* 2010). Given that the same wavelength was used for all acquisitions, Γ was retrieved through the relation (Stahl *et al* 2014):

$$\Gamma_{\text{sample}} = \frac{\left(\frac{S'_{0,\text{sample}}}{\mu_{a,\text{sample}}}\right)}{\left(\frac{S'_{0,\text{water}}}{\mu_{a,\text{water}}}\right)}\Gamma_{\text{water}} \tag{4}$$

where β cancels out.

Table 3. Tabulated properties in the literature versus experimental results (subscript-$_{exp}$). Table reproduced from Fonseca *et al* 2015, by permission of SPIE.

Material	T (°C)	C_p (J mol^{-1} K^{-1})	c (ms^{-1})	α_v (°C^{-1})	ρ	Z (MRayl)	Γ_{lit}	T_{exp} (°C)	$\hat{\Gamma}_{exp}$
Water	20	75.3	1482.3	20.6×10^{-5}	1	—	0.116		
	21.7	—	1487.47 Bilaniuk and Wong (1993)		1		0.12	21.7 ± 0.1	—
Ethanol	20	112.3	1159	140×10^{-5}	0.7893	0.91	0.772	21.5 ± 0.2	0.78 ± 0.04
Methanol	20	81.1	1116	149×10^{-5}	0.7917	0.88	0.733	19.9 ± 0.3	0.71 ± 0.02
PVCP	20	—	1402 $_{(exp)}$	—	1.008 $_{(exp)}$	1.41 $_{(exp)}$	—	21.9 ± 0.1	1.01 ± 0.05

Note. All literature values taken from Haynes (2012) unless otherwise indicated. T—temperature; C_p—specific heat capacity at constant pressure; c—sound speed; α_v—volume thermal expansion coefficient; ρ—specific gravity; Z—acoustic impedance $Z = \rho c$; Γ_{lit}—Literature-derived Grüneisen coefficient $\Gamma = \alpha_v c^2 / C_p$; $\hat{\Gamma}_{exp}$—Estimated Grüneisen coefficient.

Experiments showed that there was a negligible change in Grüneisen parameter with pigment addition up to 2%v/v (data not shown, see Fonseca *et al* (2015)).

7. Phantom imaging for various constructs

To establish feasible manufacturing strategies and configurations for PVCP, three simple phantoms were developed. These were made with soft PVCP with 0.5 mg ml^{-1} of TiO_2 (Sigma Aldrich, Germany), into a purchased silicone mould with 39 mm diameter cylindrical pockets. The motifs embedded were respectively: a simple sub-500 μm-wide line made of self-adhesive black vinyl film; a 'UCL' pattern made of self-adhesive black vinyl film; a pair of 2 mm thick soft PVCP square inserts with 2% and 8%v/v black pigment respectively. In terms of manufacture, a first layer of PVCP was poured and allowed to cure, on which the inserts of interest were then placed (figure 9). A second layer of PVCP was then deposited to fully encapsulate the inserts and allowed to cure.

Photoacoustic imaging was performed using a Fabry–Pérot scanner system (Zhang *et al* 2008), with forward mode illumination at 500 nm being provided by an OPO system providing 6 ns pulses at 30 Hz (SpitLight 600, Innolas, Krailling, Germany). The beam diameter was approximately 1 cm. Imaging parameters were: spatial resolution of $dx = 200$ μm, $dy = 200$ μm, $dt = 4$ ns, field of view $Nx \times Ny = 24 \times 22$ mm. A k-space back-projection algorithm (Treeby and Cox 2010) was used to reconstruct a 3D image of the initial pressure field from each set of acquired data. Speed of sound was set to $c = 1402\,\mathrm{ms}^{-1}$ and acoustic attenuation was not accounted for.

The reconstructed images obtained with the insert-embedded phantoms are shown in figure 10 as x–y maximum-intensity projections (where the z-axis represents the depth direction). The main features can be perceived in all phantoms.

Given that PVCP is not prone to water absorption, it is also possible to create PVCP phantoms with wall-less channels (Bykov *et al* 2010, Vogt *et al* 2015a). This is advantageous since the characteristics of the absorbing regions of interest can be easily changed between experiments, by changing the injected dye or pigment. Fewer reconstruction artefacts will also be present when compared to phantoms with walled-channels (where the wall is a different material such as a polyethylene tube), unless the wall material is explicitly accounted for. A double-channelled phantom was built to illustrate its potential use for multiple wavelength PAI. A silicone mould was used, with two 1 mm needles traversing it. After PVCP was poured and cured, the needles were removed, leaving two 1 mm diameter channels in the sample that were then filled with a solution of 34.7 g l^{-1} copper chloride ($CuCl_2{\cdot}[2H_2O]$) and 440.6 g l^{-1} nickel chloride ($NiCl_2{\cdot}[6H_2O]$) respectively. Their spectra were evaluated with the spectrophotometer.

Photoacoustic imaging was performed in similar conditions as above. Imaging parameters were: spatial resolution of $dx = 100$ μm, $dy = 100$ μm, $dt = 4$ ns, field of view $Nx \times Ny \times Nt = 15\,\mathrm{mm} \times 15\,\mathrm{mm} \times 18$ μs. Images were in this case acquired at multiple wavelengths, from 750 to 1000 nm in steps of 50 nm. Incident fluence variations with time and wavelength were corrected for. x–y and y–z maximum-intensity projection (MIP)s are shown in figures 11(a) and (b) respectively. Figures 11(c) and (d) compare the 850 nm normalised absorption spectrum measured in the spectrophotometer to a metric on the total intensity inside the tubes, found through a thresholding operation. The spectra are distinct, which is expected due to the effect of spectral colouring, to the reconstruction artefacts partially associated to limited-view and to the limitations in the accuracy of the tube segmentation and choice of total intensity as a metric.

Figure 9. Phantoms are shown before the second layer of PVCP was poured.

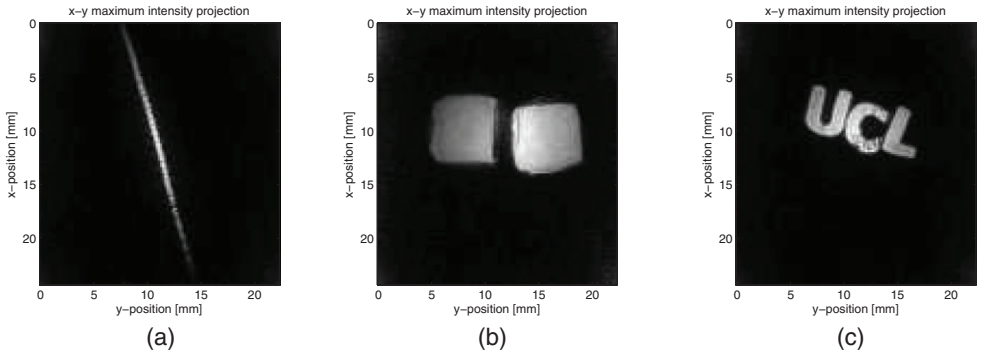

Figure 10. *x–y* maximum intensity projections of the obtained PA images. In (b), the 2%v/v and 8%v/v black PVCP inserts are positioned left and right respectively. (a) Line phantom. (b) Embedded squares phantom. (c) 'UCL' phantom.

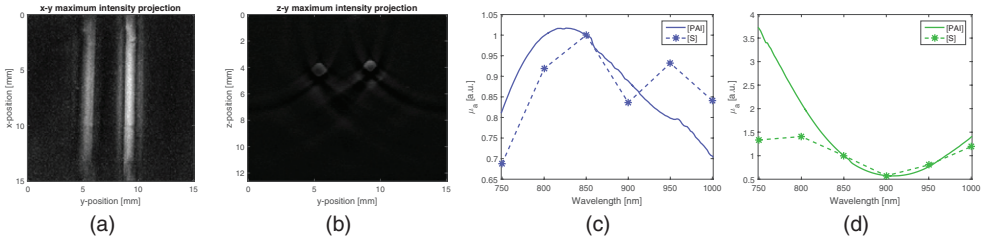

Figure 11. (a) *x–y* MIP of a 3 mm slice for the channelled phantom, at 850 nm. Left: $CuCl_2$; right: $NiCl_2$; (b) *y–z* MIP of the central 1 mm portion; (c)–(d) 850 nm normalised spectra for $CuCl_2$ and $NiCl_2$ respectively, comparing the spectrophotometer result ([S]) with the PAI intensity result ([PAI]).

8. Discussion and conclusions

As mentioned in the introduction, a qPAI algorithm must give accurate estimates with low uncertainty, be applicable in various situations, and be robust to experimental uncertainties and noise. Its validity should be demonstrated over the full range of scenarios in which the method will be applied. Many of the reported qPAI strategies have not yet assessed or met all these criteria. Studies with phantoms with realistic and known properties would be very valuable for state-of-art qPAI propositions that have only yet been implemented and tested

in simulation and that wish to extend their scope and optimise their performance in experimental scenarios (Saratoon *et al* 2013, Pulkkinen *et al* 2014, Shao *et al* 2014, Gao *et al* 2015). Likewise, phantom assessment would be of great aid to *in vivo* studies that have directly applied quantification algorithms of varying degrees of complexity and wish to assess their robustness, uncertainty and range of validity (Wilson *et al* 2014, Gottschalk *et al* 2015, Li *et al* 2016). With the advent of increasingly faster and higher resolution instrumentation (Deán-Ben *et al* 2015, Huynh *et al* 2016), as well as increasingly complex and efficient theoretical algorithms that allow high-dimensional and fine-resolution quantification both at single (Gao *et al* 2011, Saratoon *et al* 2013, Tarvainen *et al* 2014) and multiple wavelengths (Pulkkinen *et al* 2014), the need to find a phantom that is well controlled, characterised, tuneable and spatially-detailed is even more pressing and desirable.

In this paper, PVCP was characterised as a phantom material for qPAI assessment and validation studies. Its acoustic properties were assessed up to 15–20 MHz. Sound speed $c(1\text{ MHz}) = [1402.3\text{–}1408.3]\,\text{ms}^{-1}$ was within ~10% of soft tissue values and acoustic attenuation $\alpha(f) = [0.55\text{–}0.67]f^{[1.53-1.55]}$ dB cm^{-1} MHz^{-1} was analogous to soft tissues in the low frequency range, though higher than desired at increasing frequencies for most tissues except breast—as shown by the power law parameter $b = [1.53\text{–}1.55]$. This sharp frequency-dependent behaviour may pose an issue given that many structures of interest in PAI generate characteristically high frequencies. Studies by Vogt *et al* (2016) have recently shown promise in finding alternative PVCP formulations—by varying the type of plasticiser used to disperse the PVC particles—that may provide more reasonable and tailored acoustic properties.

Intrinsic optical absorption and reduced scattering with added TiO_2 as a scatterer were characterised between 400–2000 nm, corresponding to the full range of wavelengths that would be available in a typical OPO source for photoacoustics. Intrinsic absorption in the 400–1000 nm range was similar in magnitude to typical tissue background levels, around ~10^{-2} mm^{-1} order of magnitude, with higher absorption peaks above 1000 nm. Namely, the main peak at 1720 nm was made use of when performing the Grüneisen parameter characterisation. The reduced scattering was successfully tuned to tissue equivalent levels, around ~1 mm^{-1} order of magnitude.

Optical characterisation of three different absorbing pigments dispersed in PVCP revealed that they all displayed absorption linearity with concentration and distinct optical spectra, favouring their use as endogenous chromophore analogues. Nevertheless, further experiments focussing on the absorption behaviour at high peak power revealed differences compared to continuous-wave characterisation, possibly attributable to saturable absorption caused by ground-state depletion in the high-peak power regime (Piletic *et al* 2010). Since PA employs high peak power, absorber characterisation—including concentration linearity—for qPAI should always be done in this regime. The pigments displayed μ_a linearity with concentration even at high peak power. As for variation with incident peak power, the application may determine whether the variation is acceptable or not. In this study, a 5-fold variation in peak power led to up to about 13% variation in μ_a under the worst case scenario of direct surface incidence on the pigments. For the more realistic imaging phantom case of absorbing inserts at greater depth, where light has been attenuated and diffused, the variation is likely to be much less pronounced (as fluence lowers less saturable absorption phenomena occur—as seen in figure 7(f)) where the μ_a variation with fluence plateaus).

If a more stable absorption is required, one option is to explore different pigments. The particular pigments studied in this work were chosen to ensure compatibility to the matrix and resistance to the high temperature fabrication process—having come from the supplier as the PVCP—, nevertheless there is scope to explore in a wider-ranging photostability study pigments from different suppliers in the plastic materials colouring industry (Berins 1991, Pigments and Additives Division: Clariant International Ltd 2007). The main hurdle is short-listing the most

promising variants from the large repository of colourants, especially since the type of tabulated features (such as hue, light and weather fastness, fastness to bleeding, tinting strength, particle size distribution, pigment dispersibility and minimum limiting concentration) do not give direct indication about their better or worse propensity for absorption non-linearities. The photostability assessment could in a first stage be done by comparing the behaviour of the absorbing species at low and high peak power, and by exploring the behaviour at high peak power as a function of concentration, time and power (Laufer *et al* 2010, Stahl *et al* 2014), as done in this study. For a more thorough and quantifiable characterisation between distinct and concurrent non-linear photophysical phenomena such as ground-state depletion, stimulated emission and excited state absorption (Alfano 2012), techniques such as pump–probe (time-resolved) spectroscopy could be employed (Piletic *et al* 2010, Märk *et al* 2015). These characterisation studies of various absorbers are not only important if a fully-characterised, stable and reliable qPAI phantom is desired, but also for *in vivo* studies, where a thorough knowledge of the photochemical and photophysical behaviour of the endogenous or exogenous chromophores of interest at high peak power is essential. Another option to create a phantom with more stable absorption is to use a PVCP phantom with wall-less channels filled with stable and well-characterised absorbing solutions, since this will circumvent the need to disperse absorbers in PVCP directly, with added advantages that a more vasculature-realistic geometry is achieved and that the absorbers can be changed quickly by flushing the solutions in and out the channels. The use of channelled phantoms was illustrated here by performing 3D multiple wavelength PAI.

Besides the channelled phantoms, fabricating and imaging (at a single-wavelength) different geometries with various embedded structures was also possible, showing the versatility of the material.

The Grüneisen parameter was characterised to be $\Gamma = 1.01 \pm 0.05$ for the soft formulation, its high value being beneficial in yielding a high SNR in qPAI acquisitions. Changes with increasing absorber concentration were not significant.

The final conclusion is that PVCP does have the potential to be a useful and versatile phantom material for qPAI, but for now its acoustic absorption may limit its use to lower frequency (larger scale) systems, and care must be taken because of the possibility of nonlinear optical behaviour at high peak powers for some absorbers.

Acknowledgments

The work presented was supported by a CASE studentship (grant EP/L505717/1) jointly funded by the UK's Engineering and Physical Sciences Research Council and National Physical Laboratory.

The authors would like to thank N Sadhoo for guidance on using the through-transmission substitution setup available at NPL.

References

Alfano R 2012 *Biological Events Probed by Ultrafast Laser Spectroscopy* (Amsterdam: Elsevier)
Avigo C *et al* 2015 Organosilicon phantom for photoacoustic imaging *J. Biomed. Opt.* **20** 046008
Azhari H 2010 Appendix A—typical acoustic properties of tissues *Basics of Biomedical Ultrasound for Engineers* (Hoboken, NJ: Wiley) pp 313–4
Beard P 2011 Biomedical photoacoustic imaging *Interface Focus* **1** 602–31
Berera R, van Grondelle R and Kennis J 2009 Ultrafast transient absorption spectroscopy: principles and application to photosynthetic systems *Photosynth. Res.* **101** 105–18

Berins M 1991 *Plastics Engineering Handbook Of The Society Of The Plastics Industry* (New York: Springer) (https://books.google.co.uk/books?id=FzPEJyDTqtEC)
Bilaniuk N and Wong G S K 1993 Speed of sound in pure water as a function of temperature *J. Acoust. Soc. Am.* **93** 1609–12
Bohndiek S E, Bodapati S, Van De Sompel D, Kothapalli S R and Gambhir S S 2013 Development and application of stable phantoms for the evaluation of photoacoustic imaging instruments *PloS One* **8** e75533
Bykov A V, Popov A P, Kinnunen M, Prykäri T, Priezzhev A V and Myllylä R 2010 Skin phantoms with realistic vessel structure for OCT measurements *Proc. of SPIE* vol 7376 73760F
Bykov A V, Popov A P, Priezzhev A V and Myllyla R 2011 Multilayer tissue phantoms with embedded capillary system for OCT and DOCT imaging *Proc. of SPIE-OSA Biomedical Optics* vol 8091 80911R
Cook J R, Bouchard R R and Emelianov S Y 2011 Tissue-mimicking phantoms for photoacoustic and ultrasonic imaging *Biomed. Opt. Express* **2** 3193–206
Cox B, Laufer J G, Arridge S R and Beard P C 2012 Quantitative spectroscopic photoacoustic imaging: a review *J. Biomed. Opt.* **17** 061202
Cox B T, Arridge S R and Beard P C 2009 Estimating chromophore distributions from multiwavelength photoacoustic images *J. Opt. Soc. Am.* **26** 443–55
Culjat M O, Goldenberg D, Tewari P and Singh R S 2010 A review of tissue substitutes for ultrasound imaging *Ultrasound Med. Biol.* **36** 861–73
Deán-Ben X L, Ford S J and Razansky D 2015 High-frame rate four dimensional optoacoustic tomography enables visualization of cardiovascular dynamics and mouse heart perfusion *Sci. Rep.* **5** 13240
Duck F 1990 *Physical Properties of Tissue: a Comprehensive Reference Book* (San Diego, CA: Academic) (doi: 10.1118/1.596734)
Firbank M, Oda M and Delpy D T 1995 An improved design for a stable and reproducible phantom material for use in near-infrared spectroscopy and imaging *Phys. Med. Biol.* **40** 955–61
Fonseca M, Zeqiri B, Beard P and Cox B 2015 Characterisation of a PVCP based tissue-mimicking phantom for quantitative photoacoustic imaging *Proc SPIE: Opto-Acoustic Methods and Applications in Biophotonics II* **9539** 953911
Gao H, Feng J and Song L 2015 Limited-view multi-source quantitative photoacoustic tomography *Inverse Problems* **31** 065004
Gao H, Zhao H and Osher S 2011 Quantitative photoacoustic tomography *UCLA CAM Report* 11–28
Goddu R F and Delker D A 1960 Spectra-structure correlations for near-infrared region *Anal. Chem.* **32** 140–1
Gottschalk S, Fehm T F, Deán-Ben X L and Razansky D 2015 Noninvasive real-time visualization of multiple cerebral hemodynamic parameters in whole mouse brains using five-dimensional optoacoustic tomography *J. Cerebral Blood Flow Metab.* **35** 531–5
Haynes W 2012 *CRC Handbook of Chemistry and Physics* 93rd edn (London: Taylor & Francis) (http://books.google.co.uk/books?id=-BzP7Rkl7WkC)
Hungr N, Long J A, Beix V and Troccaz J 2012 A realistic deformable prostate phantom for multimodal imaging and needle-insertion procedures *Med. Phys.* **39** 2031–41
Huynh N, Zhang E Z, Betcke M, Arrridge S, Beard P C and Cox B 2016 Single-pixel optical camera for video rate ultrasonic imaging *Optica* **3** 26–29
Jacques S L 2013 Optical properties of biological tissues: a review *Phys. Med. Biol.* **58** 5007–8
Khairutdinov R F and Serpone N 1995 Laser-induced light attenuation in solutions of porphyrin aggregates *J. Phys. Chem.* **99** 11952–8
Kharine A, Manohar S, Seeton R, Kolkman R G M, Bolt R A, Steenbergen W and de Mul F F M 2003 Poly(vinyl alcohol) gels for use as tissue phantoms in photoacoustic mammography *Phys. Med. Biol.* **48** 357–70
Kislyakov I M and Yelleswarapu C S 2013 Nonlinear scattering studies of carbon black suspensions using photoacoustic Z-scan technique *Appl. Phys. Lett.* **103** 151104
Laufer J, Delpy D, Elwell C and Beard P 2007 Quantitative spatially resolved measurement of tissue chromophore concentrations using photoacoustic spectroscopy: application to the measurement of blood oxygenation and haemoglobin concentration *Phys. Med. Biol.* **52** 141–68
Laufer J, Zhang E and Beard P 2010 Evaluation of absorbing chromophores used in tissue phantoms for quantitative photoacoustic spectroscopy and imaging *IEEE J. Sel. Top. Quantum Electron.* **16** 600–7

Li R, Phillips E, Wang P, Goergen C J and Cheng J X 2016 Label-free *in vivo* imaging of peripheral nerve by multispectral photoacoustic tomography *J. Biophoton.* **9** 124–8
Luke G P, Yeager D and Emelianov S Y 2012 Biomedical applications of photoacoustic imaging with exogenous contrast agents *Ann. Biomed. Eng.* **40** 422–37
Madsen E L, Frank G R, Krouskop T A, Varghese T, Kallel F and Ophir J 2003 Tissue-mimicking oil-in-gelatin dispersions for use in heterogeneous elastography phantoms *Ultrason. Imaging* **25** 17–38
Mamonov A V and Ren K 2014 Quantitative photoacoustic imaging in the radiative transport regime *Commun. Math. Sci.* **12** 201–34
Marcano O A, Melikechi N and Verde G 2000 Shift of the absorption spectrum of organic dyes due to saturation *J. Chem. Phys.* **113** 5830
Märk J, Schmitt F J, Theiss C, Dortay H, Friedrich T and Laufer J 2015 Photoacoustic imaging of fluorophores using pump–probe excitation *Biomed. Opt. Express* **6** 2522–35
Palmer K F and Williams D 1974 Optical properties of water in the near infrared *J. Opt. Soc. Am.* **64** 1107–10
Phillips W and Griffen D 1981 *Optical Mineralogy: the Nonopaque Minerals* (San Francisco, CA: Freeman)
Pigments and Additives Division: Clariant International Ltd 2007 The coloration of plastics and rubber *Technical Report*
Piletic I R, Matthews T E and Warren W S 2010 Probing near-infrared photorelaxation pathways in eumelanins and pheomelanins *J. Phys. Chem.* A **114** 11483–91
Pinkerton J M M 1949 The absorption of ultrasonic waves in liquids and its relation to molecular constitution *Proc. Phys. Soc.* B **62** 129
Pogue B W and Patterson M S 2006 Review of tissue simulating phantoms for optical spectroscopy, imaging and dosimetry *J. Biomed. Opt.* **11** 041102
Prahl S A, van Gemert M J C and Welch A J 1993 Determining the optical properties of turbid media by using the adding-doubling method *Appl. Opt.* **32** 559
Pulkkinen A, Cox B T, Arridge S R, Kaipio J P and Tarvainen T 2014 A Bayesian approach to spectral quantitative photoacoustic tomography *Inverse Problems* **30** 065012
Saratoon T, Tarvainen T, Arridge S R and Cox B T 2013 3D quantitative photoacoustic tomography using the δ-Eddington approximation *Proc. SPIE, Photons Plus Ultrasound* **8581** 85810V
Shao P, Harrison T J and Zemp R J 2014 Consecutively reconstructing absorption and scattering distributions in turbid media with multiple-illumination photoacoustic tomography *J. Biomed. Opt.* **19** 126009
Spirou G M, Oraevsky A A, Vitkin I A and Whelan W M 2005 Optical and acoustic properties at 1064 nm of polyvinyl chloride-plastisol for use as a tissue phantom in biomedical optoacoustics *Phys. Med. Biol.* **50** N141–53
Stahl T, Allen T and Beard P 2014 Characterization of the thermalisation efficiency and photostability of photoacoustic contrast agents *Proc. of SPIE* vol 8943 p 89435H
Tarvainen T, Arridge S R, Cox B T, Kaipio J P, Kolehmainen V and Pulkkinen A 2014 Approximate marginalization of unknown scattering in quantitative photoacoustic tomography *Inverse Problems and Imaging* **8** 811–29
Treeby B E and Cox B T 2010 k-Wave: MATLAB toolbox for the simulation and reconstruction of photoacoustic wave fields *J. Biomed. Opt.* **15** 021314
Tsou J, Liu J, Barakat A I and Insana M F 2008 Role of ultrasonic shear rate estimation errors in assessing inflammatory response and vascular risk *Ultrasound Med. Biol.* **34** 2522–35
UKAS 2012 The expression of uncertainty and confidence in measurement *Technical Report*
Van de Ven J D and Erdman A G 2006 Near-infrared laser absorption of poly(vinyl chloride) at elevated temperatures *J. Vinyl Additive Technol.* **12** 166–73
Vogt W C, Jia C, Wear K A, Garra B S and Joshua Pfefer T 2016 Biologically relevant photoacoustic imaging phantoms with tunable optical and acoustic properties *J. Biomed. Opt.* **21** 101405
Vogt W C, Jia C, Wear K A, Garra B S and Pfefer J 2015a Design and phantom-based validation of a bimodal ultrasound-photoacoustic imaging system for spectral detection of optical biomarkers *Proc. of SPIE* vol 9315 p 931502
Vogt W C, Jia C, Wear K A, Garra B S and Pfefer J 2015b Quantitative assessment of photoacoustic tomography systems integrating clinical ultrasound transducers using novel tissue-simulating phantoms *Proc. of SPIE, Photons Plus Ultrasound: Imaging and Sensing* **9323** 932333
Wilson K E, Bachawal S V, Tian L and Willmann J K 2014 Multiparametric spectroscopic photoacoustic imaging of breast cancer development in a transgenic mouse model *Theranostics* **4** 1062–71

Wróbel M S, Popov A P, Bykov A V, Kinnunen M, Jedrzejewska-Szczerska M and Tuchin V V 2015 Measurements of fundamental properties of homogeneous tissue phantoms *J. Biomed. Opt.* **20** 045004

Xia W, Piras D, Heijblom M, Steenbergen W, van Leeuwen T G and Manohar S 2011 Poly(vinyl alcohol) gels as photoacoustic breast phantoms revisited *J. Biomed. Opt.* **16** 075002

Yao D k, Zhang C, Maslov K and Wang L V 2014 Photoacoustic measurement of the Grüneisen parameter of tissue *J. Biomed. Opt.* **19** 017007

Zemp R J 2010 Quantitative photoacoustic tomography with multiple optical sources *Appl. Opt.* **49** 3566–72

Zeqiri B, Scholl W and Robinson S P 2010 Measurement and testing of the acoustic properties of materials: a review *Metrologia* **47** S156–71

Zhang E, Laufer J and Beard P 2008 Backward-mode multiwavelength photoacoustic scanner using a planar Fabry–Pérot polymer film ultrasound sensor for high-resolution three-dimensional imaging of biological tissues *Appl. Opt.* **47** 561–77

Zimmermann K and Smith J 1983 Ultrasound velocity in fixed human liver: empirical anova and regression modelling on histologically assessed abnormalities *Ultrason. Imaging* **5** 280–94